Model-independent error analysis of K^+-nucleus elastic scattering

J. D. Lumpe and L. Ray
Department of Physics, The University of Texas at Austin, Austin, Texas 78712
(Received 17 June 1985)

Recent studies have demonstrated the enhanced sensitivity of K^+ mesons to interior nuclear matter distributions compared to that of protons at similar momenta. An approximately model-independent error analysis technique, similar to that used in analyses of electron scattering data, has been applied to K^+-nucleus elastic scattering at 442 and 991 MeV. The primary result of this work is that the momentum transfer range and statistical quality of data necessary to provide meaningful new constraints on the distribution of nuclear matter in the interior of large nuclei is specified. The model dependence of this approach for hadron-nucleus scattering is considered and shown to be negligible.

I. INTRODUCTION

Recently several studies[1-3] have demonstrated the enhanced sensitivity of intermediate energy K^+ mesons to interior nuclear structure properties compared to that attainable with other strongly interacting projectiles, such as intermediate energy protons.[4] The increased penetrability of the K^+ meson into nuclear matter follows directly from the relatively weak (10—20 mb) K^+ meson-nucleon (K^+N) total cross sections.[5-10] Various parameter-free, theoretical models[1,2,11,12] provide qualitative, although not as yet quantitative, descriptions of the available K^+ meson-nucleus (K^+A) scattering data.[12] For example local, coordinate space Kerman, McManus, and Thaler (KMT) (Ref. 13) optical potential models as well as Kisslinger-type nonlocal optical potentials[1,12] with densities fixed from electron scattering and effective interactions provided by the free K^+N scattering matrix [the so-called impulse approximation (IA)],[13] predict the general trend of the 800 MeV/c $K^+ + {}^{12}C$ and ${}^{40}Ca$ elastic scattering data of Marlow *et al.*[12] but underestimate the overall magnitude of the data. Nonlocal models with phenomenological forms for the off-shell portion of the K^+N t matrix do reproduce these data.[14] Very recent relativistic calculations based on the spin 0 representation of the Kemmer-Duffin-Petiau (KDP) equation[15] and a Lorentz invariant version of the impulse approximation (the so-called relativistic impulse approximation for mesons) yield predictions for 800 MeV/c $K^+ + {}^{40}Ca$ elastic scattering which are very similar to local KMT results, when the same K^+N and density information are employed. Thus, at present, we have but a qualitative understanding of the K^+ meson-nucleus interaction; quantitative theoretical success must await future improvements in these models as well as more K^+A data.

In the mean time, as an aid in designing future experiments for existing and proposed kaon facilities,[16] it is useful to specify the momentum transfer range and quality of K^+A scattering data which will eventually be required in order to permit the determination of new and meaningful nuclear structure information (e.g., accurate neutron ground state and transition densities in the nuclear interior) once the K^+-nucleus dynamics is better understood. In the present work we augment our previous sensitivity study[2] by employing a model-independent error analysis technique[17] similar to that used in the analysis of electron scattering data.

There is an essential difference, however, between the application of this technique in electron scattering, as described in Ref. 17, and the corresponding application to K^+A scattering presented here. In the former, the projectile-target interaction is both weak and theoretically well understood. This allows the use of a perturbative approach in which the charge density is written as a sum of two terms: a reference charge density, ρ_0, which yields a good fit to the experimental data and which by assumption contains no discrete ambiguities and is essentially the true density, plus a *small* perturbation, $\delta\rho_0$, which is expanded in a relevant set of basis functions. Standard perturbation theory in the Dirac formalism provides a linear relationship between infinitesimal changes in the density and corresponding infinitesimal changes in the differential cross section. Minimization of the total χ^2 for the differential cross section constrains the coefficients of the density perturbation and permits the evaluation of the covariance matrix for these coefficients as well as error envelopes for the total charge density.

In the case of hadronic probes, such a perturbative approach cannot be justified. The nuclear *matter* density in the interior region of the nucleus is not accurately known from analysis of hadronic scattering data due to depletion of the elastic channel distorted wave function as a result of absorption effects. The elastic scattering observables are only weakly sensitive to perturbations in the interior densities, even at fairly large momentum transfer.[2] We would therefore expect that for hadrons the "perturbation" in the interior matter density, $\delta\rho_0$, would not necessarily be small compared to the reference density, ρ_0. Therefore, in order to study the effects of experimental statistical errors and momentum transfer limits on the extracted matter densities we consider scattering observables which depend linearly on the entire density. We therefore utilize the K^+A scattering amplitude and expand the entire density in a set of basis functions rather than consid-

ering the differential cross section to be a linear function of a small density perturbation. This is analogous to treating the charge form factor in electron scattering as the relevant scattering observable.

Only the case of K^+A elastic scattering is considered here; the error analysis therefore applies just to the ground state density determination. The present work provides quantitative relationships between the data quality (i.e., the range in momentum transfer space and the statistical accuracy) and the resulting statistical uncertainty in the extracted ground state matter density distributions. Systematic experimental errors and theoretical uncertainties in treating the dynamics of the interaction are not accounted for. These latter two sources of uncertainty, which depend on the specifics of the eventual data and theoretical models, should of course be included in future analyses. The applicability of this (approximately) model-independent error analysis method to hadron-nucleus scattering in general is also discussed.

In Sec. II the assumed theoretical model used to describe the K^+A elastic channel dynamics and the model-independent error analysis method are explained. Section III contains a discussion of the error analysis results for several cases; these being $K^+ + {}^{40}Ca$ at 442 and 991 MeV, $K^+ + {}^{208}Pb$ at 442 MeV, and $p + {}^{40}Ca$ at 297 MeV. A summary and some general conclusions regarding the results of this study are presented in Sec. IV.

II. THEORY

The error analysis presented here is based on the model-independent technique of Ref. 17; the reader is referred to that work for a full development of the procedure. In the following we provide a brief review of this method, with greater detail being given only where specific differences from the electron scattering case arise in applications for K^+ mesons.

It is assumed that the full nuclear matter density can be expanded in a finite Fourier-Bessel series given by,

$$\rho(r)=\sum_{i=1}^{N} C_i j_0\left[\frac{i\pi r}{R}\right]\theta(R-r)\ , \tag{1}$$

where θ requires the density to be zero beyond the cutoff radius R. We furthermore assume M experimental constraints,

$$f_\alpha=\int \phi_\alpha(r) r^2 \rho(r) dr\ , \tag{2}$$

where $\alpha=1,2,\ldots,M$, f_α is the Coulomb-distorted nuclear part of the K^+A elastic scattering amplitude, and the subscript α represents the dependence on energy and scattering angle. Corresponding to these theoretical expressions are measured experimental values $f_\alpha^{\rm expt}$ which are assumed to be normally distributed with standard deviations ϵ_α. Equation (2) defines the reaction kernel $\phi_\alpha(r)$. Because the K^+A scattering amplitude arises from the strong and somewhat absorptive K^+A optical potential, Eq. (2) and all subsequent expressions must be generalized, relative to those in Ref. 17, to account for complex quantities.

As in Ref. 17 it is convenient to define the rectangular matrix $W_{\alpha i}$,

$$W_{\alpha i}\equiv \int \phi_\alpha(r) r^2 j_0\left[\frac{i\pi r}{R}\right]\theta(R-r)dr\ , \tag{3}$$

and to introduce a quantity Δ^2, analogous to the usual χ^2, given by

$$\Delta^2=\sum_\alpha \frac{|f_\alpha^{\rm expt}-\sum_{i=1}^{N} W_{\alpha i}C_i|^2}{\epsilon_\alpha^2}\ . \tag{4}$$

The quantity ϵ_α equals $\epsilon_{R,\alpha}$ or $\epsilon_{I,\alpha}$ where $\epsilon_{R,\alpha}$ and $\epsilon_{I,\alpha}$ denote, respectively, the errors in the real and imaginary parts of the experimental scattering amplitude, assumed to be independent but equal in magnitude at a given angle. Minimizing Δ^2 subject to the normalization constraint,

$$\sum_{i=1}^{N} C_i\alpha_i = A\ , \tag{5}$$

where

$$\alpha_i\equiv 4\pi\int_0^R r^2 j_0\left[\frac{i\pi r}{R}\right]dr$$

and A is the number of target nucleons, yields a matrix equation for the optimal set of density expansion coefficients $\{C_i\}$:

$$\sum_{i=1}^{N} b_{ki}C_i+\lambda\alpha_k=d_k\ , \tag{6}$$

where $k=1,2,\ldots,N$. In Eq. (6), λ is a Lagrange multiplier,

$$d_k=\sum_\alpha \frac{2\,{\rm Re}(f_\alpha^{\rm expt*}W_{\alpha k})}{\epsilon_\alpha^2} \tag{7}$$

and

$$b_{ki}=\sum_\alpha \frac{2\,{\rm Re}(W_{\alpha k}^* W_{\alpha i})}{\epsilon_\alpha^2}\ . \tag{8}$$

Note that the symmetric matrix b depends only on the statistical errors in the data and the K^+A reaction dynamics through the kernel $\phi_\alpha(r)$, whereas the column matrix d additionally depends on the experimental measurements. By defining $C_0\equiv\lambda$, $d_0\equiv A$, $b_{0i}\equiv b_{i0}\equiv\alpha_i$ and $b_{00}\equiv 0$, Eqs. (5) and (6) may be combined in the form of a single $N+1$ by $N+1$ matrix equation:

$$\sum_{i=0}^{N} b_{ki}C_i=d_k\ . \tag{9}$$

The statistical uncertainty in the density is determined by the covariance matrix of the expansion coefficients given by,

$$\delta^2 C_{ij}=2(b^{-1})_{ij}\ .$$

Subsequently the covariance in the density becomes (for $r\le R$, $r'\le R$)

$$\langle[\rho(r)-\langle\rho(r)\rangle][\rho(r')-\langle\rho(r')\rangle]\rangle = 2\sum_{i,j=1}^{N} j_0\left[\frac{i\pi r}{R}\right] j_0\left[\frac{j\pi r'}{R}\right](b^{-1})_{ij}\ . \tag{10}$$

The density distribution error envelope,

$$\Delta\rho(r)=\langle[\rho(r)-\langle\rho(r)\rangle]^2\rangle^{1/2},$$

obtained from the diagonal elements of this function, provides the statistical error in the extracted matter density as a function of the statistical errors in the data. For hadron-nucleus scattering the situation is complicated relative to electron scattering by the dependence of the matrix b on the reaction kernel, which in turn depends on the assumed density (as shown in the following). For example, if one considers elastic scattering of electrons, for which the Born approximation is generally valid, the reaction kernel depends only on $j_0(qr)$ and the static Coulomb interaction; hence errors in the data directly determine corresponding statistical errors in the charge density. In the case of strongly interacting probes such as protons, pions, alphas, and K^+ mesons the Born approximation is never valid; therefore the kernel, and consequently $\Delta\rho(r)$, is dependent to some degree on the assumed form of the density. Numerical estimates of this model dependence for hadrons are given in the following.

The explicit form of the K^+A reaction kernel can be obtained from the standard expression for the Coulomb distorted nuclear part of the elastic scattering amplitude with relativistic kinematics,[4,18] given by

$$f_{\rm CN}(k,\theta)=-\frac{\mu_\epsilon}{2\pi\hbar^2}\int d\mathbf{r}\chi^{(-)*}_{\mathbf{k}'}(\mathbf{r})U^{\rm opt}(\mathbf{r})\Psi^{(+)}_{\mathbf{k}}(\mathbf{r}), \quad (11)$$

where $\mu_\epsilon c^2=E_P E_T/(E_P+E_T)$ is the reduced energy, E_T (E_P) is the target nucleus (projectile) total relativistic energy in the projectile-nucleus c.m. system, $\chi^{(-)*}_{\mathbf{k}'}(\mathbf{r})$ is the distorted wave function due to the full Coulomb interaction, and $\Psi^{(+)}_{\mathbf{k}}(\mathbf{r})$ is the full distorted wave function. The complete K^+A scattering amplitude is given by

$$f(k,\theta)=f_{\rm Coul}(k,\theta)+f_{\rm CN}(k,\theta),$$

where $f_{\rm Coul}$ is the pure Coulomb scattering amplitude arising from the distributed charge of the target nucleus. For the K^+A nuclear interaction we use the first-order, spin-independent KMT-IA optical potential given by[2]

$$U^{\rm opt}(\mathbf{r})=\frac{1}{(2\pi)^3}\sum_{i=\rm p,n}\int d\mathbf{q}\,e^{i\mathbf{q}\cdot\mathbf{r}}\tilde{t}_i(\mathbf{q})\tilde{\rho}_i(\mathbf{q}). \quad (12a)$$

In Eq. (12a) $\tilde{t}_i(\mathbf{q})$ is the on-shell, free K^+N t matrix in the K^+A c.m. reference frame, $\tilde{\rho}_i(\mathbf{q})$ is the nucleon density form factor, and i denotes target neutrons or protons. The form of the KMT-IA optical potential and the justification for its use in sensitivity and error analysis studies of K^+-meson-nucleus scattering are presented in Refs. 1 and 2.

The wave functions and scattering amplitudes were generated by solving the radial Schrödinger equation with relativistic kinematics given by,[2,4,18]

$$\left\{\frac{d^2}{dr^2}-\frac{l(l+1)}{r^2}-\frac{2\mu_\epsilon}{\hbar^2}[U^{\rm opt}(r)+U_{\rm Coul}(r)]+k_N^2\right\}u_l(r)=0, \quad (12b)$$

where k_N is the projectile-target c.m. wave number and $U_{\rm Coul}(r)$ is the Coulomb potential. The K^+N scattering amplitudes were generated using the $l=0$, 1, and 2 phase shifts of Martin[8] and typical tabulated phase shift values for the small, higher partial waves through $l=4$ (Refs. 9, 10, and 19). The SP82 energy-independent nucleon-nucleon (NN) phase shift solutions of Arndt *et al.*[19] provided the pN scattering amplitudes. For convenience, only the spin-independent portion of the pN amplitudes was retained. The proton densities for ^{40}Ca and ^{208}Pb were obtained from the charge densities of Refs. 20 and 21, respectively, by unfolding the single proton charge form factor and correcting for contributions to the charge density arising from the neutron's electric form factor and nucleon magnetic moments.[18,22] The Hartree-Fock-Bogoliubov (HFB) calculations of Dechargé and Gogny[23] provided the neutron densities.

In Ref. 2 it was empirically found that the 442 MeV $K^+ + {}^{40}$Ca elastic scattering data of Marlow *et al.*[12] can be accurately reproduced within the above model if one sets $t_{K^+n}=t_{K^+p}$, where t_{K^+p} is obtained from the CMK phase shift solution of Arndt.[19] It is worthwhile to note that repetition of the calculations presented in Sec. III using this resulting phenomenological optical potential as input results in error envelopes for the extracted matter densities which differ negligibly from those obtained here.

Upon substitution of Eq. (12a) into Eq. (11) the scattering amplitude becomes

$$f_{\rm CN}(k,\theta)=-\frac{\mu_\epsilon}{(2\pi)^4\hbar^2}\sum_{i=\rm p,n}\int d\mathbf{r}\,d\mathbf{q}\chi^{(-)*}_{\mathbf{k}'}(\mathbf{r})e^{i\mathbf{q}\cdot\mathbf{r}}\tilde{t}_i(\mathbf{q})\tilde{\rho}_i(\mathbf{q})\Psi^{(+)}_{\mathbf{k}}(\mathbf{r}), \quad (13a)$$

or alternatively, it can be expressed as,

$$f_{\rm CN}(k,\theta)=-\frac{\mu_\epsilon}{(2\pi)\hbar^2}\sum_{i=\rm p,n}\int d\mathbf{r}\,d\mathbf{r}'\chi^{(-)*}_{\mathbf{k}'}(\mathbf{r})t_i(|\mathbf{r}-\mathbf{r}'|)\rho_i(\mathbf{r}')\Psi^{(+)}_{\mathbf{k}}(\mathbf{r}), \quad (13b)$$

where

$$t_i(\mathbf{r})=\frac{1}{(2\pi)^3}\int d\mathbf{q}\,e^{i\mathbf{q}\cdot\mathbf{r}}\tilde{t}_i(\mathbf{q}). \quad (13c)$$

The wave functions and the K^+N t matrix are expanded as follows:

$$t_i(|\mathbf{r}-\mathbf{r}'|)=\sum_\lambda t_{\lambda,i}(r,r')P_\lambda(\hat{\mathbf{r}}\cdot\hat{\mathbf{r}}'),$$

$$\chi^{(-)*}_{\mathbf{k}'}(\mathbf{r})=\frac{4\pi}{k'r}\sum_{l_1,m_1}(-i)^{l_1}u^{\rm Coul}_{l_1}(r)Y^*_{l_1m_1}(\hat{\mathbf{r}})Y_{l_1m_1}(\hat{\mathbf{k}}'),$$

and

$$\Psi_{\mathbf{k}}^{(+)}(\mathbf{r})=\frac{4\pi}{kr}\sum_{l_2,m_2}(i)^{l_2}u_{l_2}(r)Y_{l_2m_2}(\hat{\mathbf{r}})Y^*_{l_2m_2}(\hat{\mathbf{k}})\ .$$

The radial wave function, $u_l(r)$, is obtained from Eq. (12b) and the pure Coulomb radial wave function, $u_l^{\text{Coul}}(r)$, is similarly obtained except that $U^{\text{opt}}(r)$ is set equal to zero. We then obtain the following expression for the elastic scattering amplitude for spherically symmetric targets,

$$f_{\text{CN}}(k,\theta)=-\frac{8\pi\mu_\epsilon}{(\hbar k)^2}\sum_l(2l+1)P_l(\cos\theta)\times\sum_{i=\text{p,n}}\int_0^\infty r^2\rho_i(r)\xi_{l,i}(r)dr\ , \quad (14)$$

where

$$\xi_{l,i}(r)=\int_0^\infty u_l^{\text{Coul}}(r')t_{0,i}(r,r')u_l(r')dr'\ .$$

Therefore the reaction kernel takes the explicit form

$$\phi_\alpha(r)=-\frac{8\pi\mu_\epsilon}{(\hbar k)^2}\sum_l(2l+1)P_l(\cos\theta)\times\sum_{i=\text{p,n}}\frac{\rho_i(r)}{\rho(r)}\xi_{l,i}(r)\ , \quad (15)$$

where $\rho(r)=\rho_{\text{p}}(r)+\rho_{\text{n}}(r)$ is factored out. $\phi_\alpha(r)$ depends on the pure Coulomb and full distorted wave functions and the monopole projection of the K^+N effective interaction. Note that the explicit dependence of $\phi_\alpha(r)$ on the target densities is eliminated for isoscalar effective interactions. Since the K^+A and proton-nucleus optical potentials used in this analysis are, in fact, almost purely isoscalar,[2,24] the explicit dependence of $\phi_\alpha(r)$ on target densities is minute.

In the calculations presented here uniform percent errors were assumed for the nuclear part of the elastic scattering differential cross section (given by $|f_{\text{CN}}|^2$). The set of experimental amplitude errors ϵ_α, for each case was obtained as follows. First, a standard density model with $\rho_{\text{p}}(r)$ taken from electron scattering analyses and a HFB neutron density together with projectile-nucleon elastic scattering amplitudes were combined to form the first-order, spin-independent KMT optical potential given in Eq. (12a) and discussed in Ref. 2. From this optical potential, Coulomb distorted nuclear elastic scattering amplitudes were computed for a specified set of scattering angles (50 points at 1° intervals for the standard case with $q_{\max}=3.3$ fm^{-1}; see Sec. III). Given the previous assumption that the errors in the real and imaginary parts of the nuclear scattering amplitude are independent and equal in magnitude, the result,

$$\epsilon_\alpha=\frac{1}{2}\left[\frac{\Delta\sigma}{\sigma}\right]_\alpha\left[\frac{d\sigma}{d\Omega_\alpha}\right]^{1/2}\ , \quad (16)$$

is obtained, where $(\Delta\sigma/\sigma)_\alpha$ is the assumed percent uncertainty in the nuclear portion of the differential cross section,

$$\sigma_\alpha\equiv(d\sigma/d\Omega_\alpha)=|f_{\text{CN}}|^2\ .$$

Equations (3), (8), (10), and (15) are then used to obtain the error envelopes.

The contribution of the full distorted wave function means that for K^+A scattering $\phi_\alpha(r)$ depends somewhat on the assumed target density and this manifests itself as an additional source of model dependence in the error envelopes. Because the K^+N interaction is relatively weak, the distortion of the K^+ meson wave function in the nucleus is slight and therefore we expect this model dependence to be small. It is essential that this be the case if the calculated uncertainties in the extracted densities are to be meaningfully related to the statistical errors in the data.

The extent of this additional model dependence was investigated for K^+ meson and proton projectiles in the following manner. First, the above standard density model was used to generate the density error envelopes as discussed above. This calculational procedure was repeated using an alternative neutron density model which differed from the HFB distribution by 20% in the interior. The surface geometry of this second neutron density was adjusted in order that both calculations produce similar scattering amplitudes. In the case of 442 MeV $K^+ + {}^{40}$Ca the resulting two error envelopes differ by less than 0.74×10^{-4} out of 0.24×10^{-2} nucleons/fm^3 in the interior region. For 297 MeV $p + {}^{40}$Ca the envelopes differ by 0.77×10^{-4} out of 0.63×10^{-2} nucleons/fm^3. Therefore, the density error envelopes calculated by the modified method of Ref. 17 for K^+A elastic scattering, as well as for pA elastic scattering, adequately relate experimental errors in the data to statistical uncertainty in the extracted densities without undue model dependence.

In addition to this implicit model dependence there are, by necessity, explicit model assumptions which must be specified. These involve the choice of values for the cutoff radius R, and number of terms N, in the Fourier-Bessel expansion of the density. The calculated envelopes were found to be insensitive to the value of the cutoff radius; $R=8.4$ and 11.4 fm were used for ^{40}Ca and ^{208}Pb, respectively. The number of terms used in the expansion is determined by imposing a lower limit on the minimum allowed wavelength of fluctuations in the density. Assuming this corresponds to the size of the nucleon constituents (i.e., 1.6 fm), and using the above values for R, we obtain the limits $N=10$ and 14 for ^{40}Ca and ^{208}Pb, respectively.

Note the essential difference between this method of fixing the number of terms in the expansion and that used in Ref. 17. In the latter work, the maximum momentum transfer, $q_{\max}$, is specified by the data to be analyzed. The number of Fourier-Bessel coefficients is optimized in order to achieve the minimum combined statistical and completeness error[17] in the density. In our situation $q_{\max}$, in conjunction with the experimental statistical errors, ϵ_α, are varied such that the resulting statistical uncertainty in the density lies within a desired degree of accuracy. The number of Fourier-Bessel coefficients is motivated strictly by considering the minimum realistic size of quantum fluctuations in the density. For our choice of N the completeness errors are negligible.

III. RESULTS

The standard case considered in this study was $K^+ + {}^{40}Ca$ elastic scattering at 442 MeV, corresponding to a c.m. momentum of 3.9 fm^{-1} where cross section data exist.[12] The mass and energy dependences of the error envelopes were investigated by including the cases $K^+ + {}^{208}Pb$ at 442 MeV and $K^+ + {}^{40}Ca$ at 991 MeV, respectively. Also considered was $p + {}^{40}Ca$ elastic scattering at the lower incident momentum for comparison with the K^+ meson case.

The results of the error analysis for $K^+ + {}^{40}Ca$ at 442 MeV, using the values of R and N quoted in the previous section, are shown in Fig. 1. These different error envelopes, shown as $[\Delta\rho(r)/\rho(r)]\times 100\%$, were generated by varying the maximum momentum transfer. The solid line (standard case) corresponds to $q_{max}=3.3$ fm^{-1} with uniform statistical errors of $\pm 10\%$ in the nuclear differential cross section. This yields uncertainties in the matter density which vary from $\sim 2\%$ in the interior to less than 1% on the surface, finally extending upwards to 100% in the tail region. Reducing q_{max} from 3.3 to 3.0 fm^{-1} [$M=45$ in Eq. (2)] and finally to 2.0 fm^{-1} [$M=30$ in Eq. (2)] permits larger and larger uncertainties in the higher Fourier components of the density, resulting in a characteristic oscillatory behavior in the envelopes and a large increase in their magnitude. For $q_{max}=2.0$ fm^{-1}, comparable to the best available data of Marlow *et al.*,[12] the uncertainties exceed 100% at all r since the high Fourier-Bessel terms (small wavelength oscillations) are essentially unconstrained. Therefore no *model-independent* density information can be obtained from analyses of these data. The standard case ($q_{max}=3.3$ fm^{-1}) would, however, be sufficient to provide new information about matter densities in the interior of ^{40}Ca. Error envelopes corresponding to other assumed values for the uniform statistical uncertainty in the cross section are readily obtained from the curves in Fig. 1 by noting that $\Delta\rho(r)\propto\epsilon_\alpha\propto(\Delta\sigma/\sigma)_\alpha$. Similarly, the effect on the error envelopes of choosing a different number of experimental constraints is simply determined from the relationship $\Delta\rho(r)\propto M^{-1/2}$ (given a fixed q_{max} and ϵ_α and assuming a uniform angular spacing of points).

Shown in Fig. 2 are results comparing the effect of constant statistical errors throughout the angular range of the data to the more realistic case in which statistical errors increase with larger scattering angle. The solid line represents the standard case shown in Fig. 1. The dash-dot curve results from assuming nuclear cross section errors of $\pm 5\%$ in the angular range 0°—15° c.m., $\pm 10\%$ from 15°—25° c.m., and $\pm 15\%$ from 25°—50° c.m. ($q_{max}=3.3$ fm^{-1}) where the same angular distribution of experimental constraints as in the standard case is used. The dotted curve was generated similarly, but with assumed errors of $\pm 10\%$, $\pm 15\%$, and $\pm 20\%$ in the same angular ranges, respectively. The latter envelope differs from the standard case by the maximum amount in the interior, resulting in errors $\sim 55\%$ larger than the standard case at the origin. The dash-dot curve, on the other hand, is essentially identical to the standard case at the origin but becomes smaller by a factor of $\sim 35\%$ in the

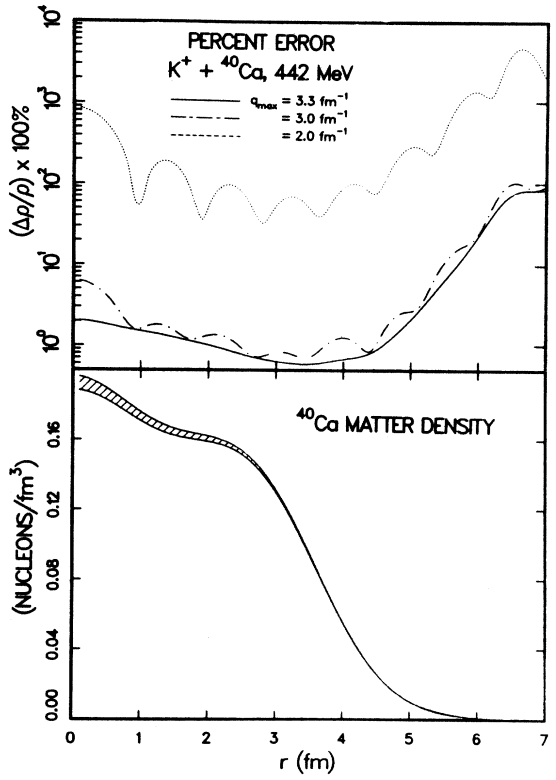

FIG. 1. Percent statistical uncertainties (i.e., $[\Delta\rho(r)/\rho(r)]\times 100\%$) in the ^{40}Ca matter density resulting from analysis of $K^+ + {}^{40}Ca$ elastic scattering at 442 MeV. The maximum momentum transfer (q_{max}) and uniform statistical error in the nuclear portion of the differential cross section are assumed to be 2.0 fm^{-1}, $\pm 10\%$ (dotted curve): 3.0 fm^{-1}, $\pm 10\%$ (dash-dot curve); and 3.3 fm^{-1}, $\pm 10\%$ (solid curve). The error envelope shown on the ^{40}Ca input matter density (lower half of figure) corresponds to the $q_{max}=3.3$ fm^{-1} case.

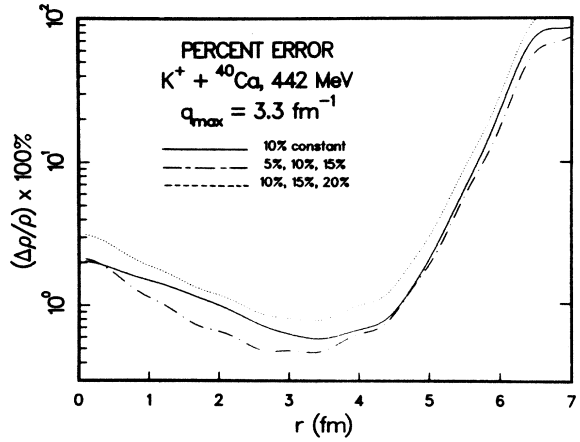

FIG. 2. Same as Fig. 1 except the dash-dot curve results from analysis with $q_{max}=3.3$ fm^{-1} and statistical errors of $\pm 5\%$ from 0°—15° c.m., $\pm 10\%$ from 15°—25° c.m., and $\pm 15\%$ from 25°—50° c.m. The dotted curve is obtained by assuming $q_{max}=3.3$ fm^{-1} with errors of $\pm 10\%$, $\pm 15\%$, and $\pm 20\%$, respectively. The solid curve is the same as in Fig. 1. The surface region of the ^{40}Ca density distribution of Fig. 1 corresponds approximately to the range $2.5 \lesssim r \lesssim 4.5$ fm.

region $1 \leq r \leq 3$ fm. Although it is desirable to minimize the experimental errors as much as possible in the high-q region in order to more effectively constrain the interior density distribution, the dotted curve indicates that data extending to ~ 3.3 fm^{-1}, even with fairly large statistical errors, can still be used to determine the interior density to less than $\pm 5\%$.

Interesting also are the mass and energy dependences of the envelopes. We expect the uncertainties in the extracted density to increase with increasing projectile energy and target mass, due to greater absorption. Above 800 MeV/c (4 fm^{-1}) incident momentum the K^+N total cross sections rise sharply as various inelastic channels, including the $K\Delta$, K^*N, and $K^*\Delta$ resonances, become energetically accessible.[5] This increased absorption should diminish the sensitivity of the K^+ meson to the interior matter distributions. Similarly, one expects a decreased sensitivity to the interiors of larger nuclei as a direct consequence of the finite mean free path of the K^+ meson in nuclear matter.

In order to determine the extent of this expected mass and energy dependence, envelopes were generated for $K^+ + {}^{40}$Ca at 991 MeV and $K^+ + {}^{208}$Pb at 442 MeV; the results are shown in Figs. 3 and 4, respectively, compared with the standard case. The higher energy corresponds to a c.m. momentum of 7 fm^{-1}. In each calculation q_{max} equals 3.3 fm^{-1} and constant statistical errors in the nuclear cross section of $\pm 10\%$ were assumed. For $K^+ + {}^{40}$Ca at 991 MeV 50 angular points at uniform intervals were used. The same angular distribution of experimental constraints was assumed for $K^+ + {}^{208}$Pb at 442 MeV as in the standard case. The higher energy $K^+ + {}^{40}$Ca analysis results in uncertainties in the density which differ significantly from the standard case only in the extreme interior ($r \leq 1$ fm), where they are at most a factor of $\sim 35\%$ larger. It is therefore still possible at this higher energy to extract meaningful information about the interior matter distributions of ^{40}Ca, provided the data extend to $q \geq 3.0$ fm^{-1} with adequate statistical accuracy. For $K^+ + {}^{208}$Pb at the lower energy, the analysis yields

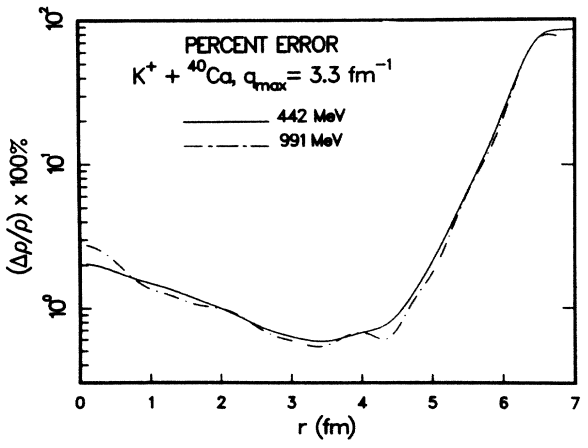

FIG. 3. The solid curve represents the standard case and is the same as in Fig. 1. The dash-dot curve results from analysis of $K^+ + {}^{40}$Ca at 991 MeV with identical q_{max} and statistical errors.

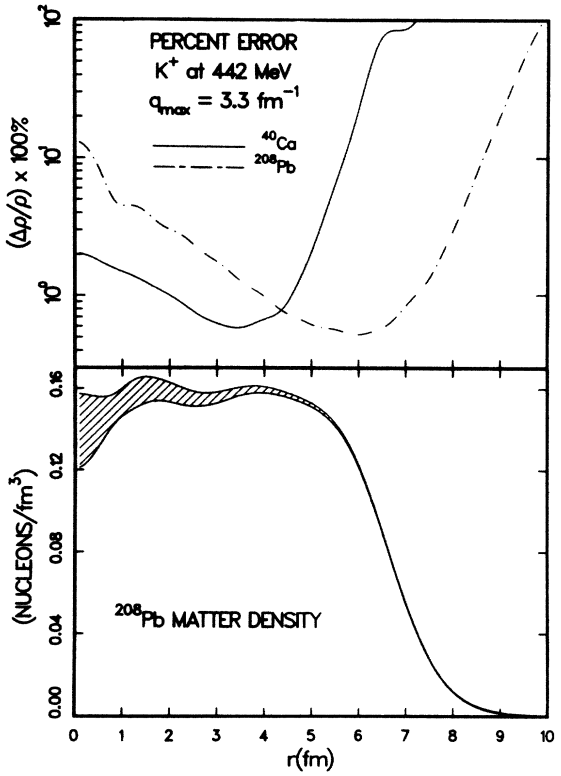

FIG. 4. Same as Fig. 3, except that the dash-dot curve results from analysis of $K^+ + {}^{208}$Pb at 442 MeV with identical q_{max} and statistical errors. The input ^{208}Pb matter density is shown with the error envelope corresponding to the dash-dot curve.

matter density error envelopes which are considerably larger than the $K^+ + {}^{40}$Ca case in the interior, being as much as $\pm 13\%$ at $r = 0$. The uncertainties in the surface and tail regions of ^{208}Pb are comparable to that for ^{40}Ca. From Fig. 4 we see that more stringent statistical errors, perhaps as low as $\pm 5\%$ in the differential cross section data, would be required in order to extract interior neutron densities for ^{208}Pb of sufficient accuracy to empirically select between various theoretical predictions, study nuclear shell structure, etc.[23,25,26]

Finally, in order to provide a relative comparison of the K^+ meson and proton projectiles, matter density error envelopes were generated for $p + {}^{40}$Ca elastic scattering at 297 MeV (3.9 fm^{-1} incident momentum), with $q_{max} = 3.3$ fm^{-1} and constant $\pm 10\%$ errors in the nuclear portion of the differential cross section (same number of angles, M, as in the standard $K^+ + {}^{40}$Ca case). The result is shown in comparison with the standard case in Fig. 5. The curves indicate that the K^+ meson results in errors which are a factor of ~ 5 smaller in the interior, whereas the two probes provide a roughly equivalent determination of the ^{40}Ca density in the surface and tail regions, $r \geq 3.5$ fm. This is consistent with the findings of the sensitivity study of Ref. 2 which concluded that the K^+ meson offered enhanced sensitivity to the matter distributions in the nuclear interior. The oscillations in the dash-dot curve result from suppressed sensitivity of the large angle data to the higher Fourier density components. This in turn is

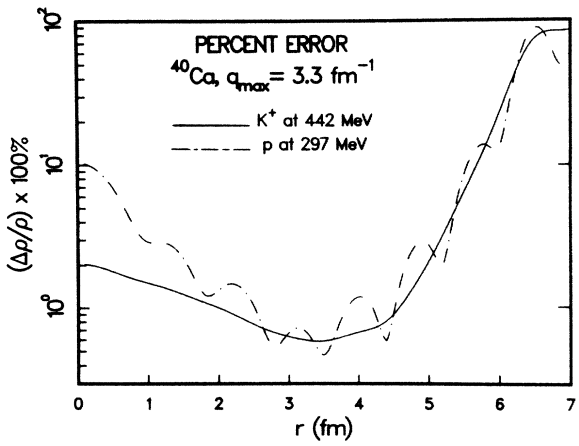

FIG. 5. Same as Fig. 3 except that the dash-dot curve results from analysis of p+^{40}Ca at 297 MeV with identical q_{max} and statistical errors.

due to the large distortions in the pA scattered wave function which permit sizable contributions of the low Fourier components of the density at large momentum transfer.

IV. SUMMARY AND CONCLUSIONS

In this work an essentially model-independent error analysis of intermediate energy K^+A elastic scattering has been performed. The purpose of this study was to specify, as realistically as possible, the minimum quality of K^+A elastic scattering data which upon careful analysis could lead to new nuclear structure information in the interiors of large nuclei. In order that this technique be applicable to hadron-nucleus scattering it is important that the computed error envelopes be minimally dependent on the assumed form of the input density. Calculations carried out here demonstrate that this requirement is satisfied for K^+A scattering and is also adequate for proton projectiles at 300 MeV.

For K$^+$ meson elastic scattering from ^{40}Ca at 442 MeV, the results indicate that differential cross section data extending to $q \geq 3.0$ fm^{-1} with statistical errors of $\pm 10\%$ would be sufficient to determine the interior neutron density to within $\pm 5\%$. Furthermore, the errors in the extracted density do not exhibit any dramatic mass or energy dependence. In particular, calculations for K$^+$ + ^{208}Pb at 442 MeV, with the same momentum transfer range and statistical quality of elastic scattering data, result in a typical uncertainty of about $\pm 7\%$ in the interior region of the ^{208}Pb neutron density distribution (about $\pm 20\%$ in the extreme interior, $r < 1$ fm).

These calculations quantitatively demonstrate the enhanced sensitivity of K$^+$ mesons to matter density distributions in the nuclear interior compared to that which can be achieved with protons.[1,2,4,27,28] However, it is important to remember that accurate nuclear matter densities cannot be obtained until high quality K^+A scattering data along with more realistic and accurate theoretical models of the K^+A reaction process are available.

This research was supported in part by the U.S. Department of Energy and the Robert A. Welch Foundation.

[1]W. R. Coker, G. W. Hoffmann, and L. Ray, Phys. Lett. **135B**, 363 (1984).
[2]W. R. Coker, J. D. Lumpe, and L. Ray, Phys. Rev. C **31**, 1412 (1985).
[3]S. R. Cotanch, Phys. Rev. C **21**, 2115 (1980); **23**, 807 (1981).
[4]L. Ray, W. R. Coker, and G. W. Hoffmann, Phys. Rev. C **18**, 2641 (1978).
[5]C. B. Dover and G. E. Walker, Phys. Rep. **89**, 1 (1982).
[6]C. B. Dover, in *Low & Intermediate Energy Kaon-Nucleon Physics,* edited by E. Ferrari and G. Violini (Reidel, Boston, 1981), p. 165.
[7]C. B. Dover and P. J. Moffa, Phys. Rev. C **16**, 1087 (1977).
[8]B. R. Martin, Nucl. Phys. **B94**, 413 (1975).
[9]B. R. Martin and C. G. Oades, Proceedings of the IV International Conference on Baryon Resonances, Toronto, 1980; and private communication.
[10]S. J. Watts *et al.*, in *Low & Intermediate Energy Kaon-Nucleon Physics,* edited by E. Ferrari and G. Violini (Reidel, Boston, 1981), p. 215.
[11]A. Chaumeaux and M.-C. Lemaire, Phys. Rev. C **28**, 772 (1983).
[12]D. Marlow *et al.*, Phys. Rev. C **25**, 2619 (1982).
[13]A. K. Kerman, H. McManus, and R. M. Thaler, Ann. Phys. (N.Y.) **8**, 551 (1959).
[14]P. B. Siegel, W. B. Kaufmann, and W. R. Gibbs, Phys. Rev. C **30**, 1256 (1984).
[15]B. C. Clark, S. Hama, G. R. Kälbermann, R. L. Mercer, and L. Ray, Phys. Rev. Lett. **55**, 592 (1985).
[16]See Los Alamos National Laboratory Report LA-UR-84-3982, 1984; LAMPF II Proposal to the U.S. Department of Energy, edited by G. T. Garvey, L. Rosen, and H. A. Thiessen; and a review of Kaon research proposals at TRIUMF is given by P. Kitching in Proceedings of the Third LAMPF II Workshop, edited by J. C. Allred, T. S. Bhatia, K. Ruminer, and B. Talley, Los Alamos National Laboratory Conference Report LA-9933-C, Vol. II, p. 548, and references therein.
[17]J. L. Friar and J. W. Negele, in *Advances in Nuclear Physics,* edited by M. Baranger and E. Vogt (Plenum, New York, 1975), Vol. 8, p. 219.
[18]L. Ray, Phys. Rev. C **19**, 1855 (1979).
[19]The pN phase shifts are taken from R. A. Arndt *et al.*, Phys. Rev. D **28**, 97 (1983) using the Virginia Polytechnic Institute scattering analysis interactive dial-in (SAID) program. The K$^+$p phase shifts are also obtained from the VPI-SAID program, solution CMK. The high partial wave K$^+$n phase shift solutions of K. Hashimoto, Phys. Rev. C **29**, 1377 (1984) were also used; these were obtained using the VPI-SAID program with solution HASH; and also K. Hashimoto, private communication.
[20]I. Sick *et al.*, Phys. Lett. **88B**, 245 (1979).
[21]B. Frois *et al.*, Phys. Rev. Lett. **38**, 152 (1977).
[22]W. Bertozzi, J. Friar, J. Heisenberg, and J. W. Negele, Phys. Lett. **41B**, 408 (1972).
[23]J. Dechargé and D. Gogny, Phys. Rev. C **21**, 1568 (1980); J. Dechargé, M. Girod, D. Gogny, and B. Grammaticos, Nucl. Phys. **A358**, 2036 (1981); J. Dechargé (private communica-

tion).
[24]L. Ray, P. C. Tandy, and R. M. Thaler, Phys. Rev. C **28**, 506 (1983).
[25]J. W. Negele and D. Vautherin, Phys. Rev. C **5**, 1472 (1972).
[26]B. Frois, in Proceedings of the International Conference on Nuclear Physics with Electromagnetic Interactions, Mainz, Federal Republic of Germany, 1979, edited by H. Arenhövel and D. Drechsel, published in *Lecture Notes in Physics* (Springer, Berlin, 1979), Vol. 108, p. 52.
[27]L. Ray *et al.*, Phys. Rev. C **23**, 828 (1981).
[28]G. W. Hoffmann *et al.*, Phys. Rev. C **21**, 1488 (1980); **24**, 541 (1981).